Journal of Computers Vol. 31 No. 5, 2020, pp. 30-43
doi:10.3966/199115992020103105003

Feature Extraction Method Based on Gray Value Star-shaped Projection

Mengyi Liao[1,2], Kun Zhang[1*], Bing Li[2], Jianfang Liu[2]

[1] National Engineering Research Center for E-Learning, Central China Normal University, Wuhan 430079, China
zhk@mail.ccnu.edu.cn

[2] College of Computer Science and Technology, Pingdingshan University, Pingdingshan 467000, China
liaomengyi83@163.com

Received 13 March 2019; Revised 18 July 2019; Accepted 28 August 2019

Abstract. Augmented reality (AR) has been widely used in the field of education, which puts forward higher performance for AR systems. The extraction of feature is the basis of implementing tracking registration in AR systems. The latest feature extraction methods cannot well meet the needs in the education field. Therefore, we propose a new feature extraction algorithm: On the basis of extracting the edge of the image, the star-shaped projection values are calculated for all the pixels in the detection area for initial extraction of features. Then the false features are gradually eliminated by judging the main peak areas and the distance between two main peaks. Finally, binary robust independent elementary features (BRIEF) descriptor is used to describe features and hamming distance is used to match features. The experimental results show that, the average time of feature matching in this paper is only 22% of the improved speed up robust features (SURF) algorithm, and 87% of the improved oriented rotated BRIEF (ORB) algorithm. The correct matching rate of the features is higher than both improved SURF and improved ORB in the case of illumination variation, scale variation and visual angle variation.

Keywords: augmented reality, feature extraction, gray value, star-shaped projection

1 Introduction

AR is a technology that combines computer-generated virtual objects with real environments to augment real scenes [1]. In 2016, Horizon Report released by the New Media Consortium of the United States listed AR as a technology that would have an important impact on education and teaching in the future. As an effective technology for integrating digital teaching resources with the real world, AR is widely used in various learning situations such as game learning, inquiry learning and collaborative learning, especially in the education field of special children, who have impairments in hearing, intelligence, social communication or language ability. The AR learning environment can greatly enhance educational effects by its unique narrative method, interaction strategy and collaborative communication environment [2]. At the same time, due to the diversity of teaching scenarios and interaction modes [3], higher performance requirements are imposed on real-time, scale invariance and rotation invariance of AR system.

Tracking registration is the core technology of AR, and the extraction of features is the basis of tracking registration and influence the speed and accuracy of tracking registration [4]. In recent years, a large number of feature extraction methods have emerged, and they can be classified into three categories: feature extraction based on contour curve, such as curvature scale space (CSS) algorithm [5]; feature extraction based on gray-scale image, such as SURF algorithm and ORB algorithm [6-7]; feature extraction based on template, such as features from accelerated segment test (FAST) algorithm [8-10].

* Corresponding Author

Among them, the algorithms based on template have higher detection efficiency and rotation invariance, but cannot adapt to noise and strong light interference. The algorithms based on contour curve can improve the position accuracy of features, but it doesn't have scale invariance, which is easy to cause false detection [11]. At present, most of the researches focus on the methods based on gray-scale image. David et al. [12] proposed a method based on scale-invariant feature transform (SIFT), which improved the accuracy of feature matching, but the efficiency of time and space were low. Compared with the SIFT, Bay et al. [13] proposed a new feature extraction method based on SURF, the speed of feature extraction was improved, but the floating point descriptor vector was used with large memory consumption. Rublee et al. [14] proposed the ORB feature extraction method, which had higher computational speed, stronger anti-noise ability and rotational invariance, but this method did not have scale invariance. In view of the limitations of the above methods, researchers have proposed some improved methods. JU et al. [6] proposed an improved SURF algorithm, which can match the features in real-time in the case of scale variation. GONG et al. [7] proposed an improved ORB algorithm to improve the matching performance of features under different illumination conditions. These methods improved the performances without taking into account all factors that change the image quality. Therefore, according to the high performance requirements of augmented reality learning environment, a new feature extraction method based on gray value star-shaped projection is proposed, which performs well in case of angle variation, illumination variation, scale variation. Using star-shaped projection of gray value magnifies the difference of gray values and improves the robustness of the algorithm. What's more, in this method, the adaptive extraction threshold is set to improve the efficiency of the algorithm and the user experience.

To promote efficiency and robustness of feature extraction, a new feature extraction method based on gray value star-shaped projection is proposed in this paper. Our method combines the merits of gray-scale-based and contour curve-based approaches. It offers more reliable recognition results and better robustness than its competitors. Our algorithm includes three key steps: (i) extracting the edge of image and performing the star-shaped projection on the edge points and (ii) finding the main peak area and the main peak distance and (iii) judging the features through the main peak area and the main peak distance. The advantages of our method can be summarized as follows:

- It adopts an adaptive extraction threshold to improve the efficiency of the algorithm.
- It offers better robustness through magnifying the difference of gray values in the projection area.
- It can eliminate false features by judging the main peak areas and the main peak distance.

The paper is organized as follows. Section 1 introduces the development of feature extraction methods and the application background. In section 2, the new method based on gray value star-shaped projection was proposed. Section 3 verifies the performance of our algorithm and other algorithms using videos taken in the natural scene and two popular image sets. Our algorithm is also applied to the augmented reality system developed to improve children's cognitive ability. Finally, in section 4, conclusion is given.

2 The Proposed Method

Firstly, Gaussian Laplacian algorithm is used to extract the edge of image in the proposed method. On the basis of edge detection, the star-shaped projection is performed on the edge points that meet the extraction threshold of the center point to magnify the difference of gray values in the projection area. Then, the position of center point is located initially by image thinning. Next, the main peak area and the main peak distance are calculated, and the center point is judged as features or false features through the main peak distance. What's more, feature description is performed with BRIEF descriptor and feature matching is performed with Hamming distance.

2.1 Gaussian Laplacian Algorithm for Image Edge Extraction

In an image, edges of objects contain important shape information and semantic information. The image can be quickly identified through edge detection. Usually, features exist at the intersection points of the object edges in the image, so extracting the edges of the image are the basis of features extraction [15]. The object edge in the image is a part of the pixels which has a sudden change in the gray value. The gray value of the edge pixel has variability compared with the gray value of the adjacent pixel [16]. Based on these characteristics, Gaussian Laplacian algorithm is used in this paper to extract image edges. The edge points and noise points in an image are at similar frequency values, as a result, when we extract

the edges, the noise points are inevitably extracted at the same time. The extraction of noise points greatly affects the accuracy and efficiency of features extraction, so smoothing filter is required to filter the noise points before edge extraction.

In this paper, the Gaussian filter is used to smooth the image. It uses the convolution operation to relatively average the gray values of the adjacent pixels in the image to reduce the influence of the noise points and the contrast of the image. The weights of convolution operation at different positions are determined according to the location of the adjacent points and the center points [17]. According to the two-dimensional separability of the Gaussian filter, the operation can be performed as shown in formula (1):

$$\frac{1}{16}\begin{bmatrix}1 & 2 & 1\\ 2 & 4 & 2\\ 1 & 2 & 1\end{bmatrix}=\frac{1}{16}\begin{bmatrix}1\\ 2\\ 1\end{bmatrix}\times\begin{bmatrix}1 & 2 & 1\end{bmatrix}. \tag{1}$$

The Laplacian is the simplest isotropic differential operator with rotation invariance. The Laplace transform of a two-dimensional image is an isotropic second-order derivative, defined as:

$$\nabla^2 f(x,y)=\frac{\partial^2 f}{\partial x^2}+\frac{\partial^2 f}{\partial y^2}. \tag{2}$$

In order to improve the efficiency of digital image processing, formula (2) can be converted as follows:

$$\nabla^2 f=[f(x+1,y)+f(x-1,y)+f(x,y+1)+f(x,y-1)]-4f(x,y). \tag{3}$$

Through the above formula, the result of Laplacian of one pixel is the sum of the gray values of the adjacent pixels of the upper, lower, left and right minus four times the gray value of itself, as shown in Fig. 1(a). Fig. 1(a) is a four-adjacent Laplacian operator. After it is rotated by 45°and added to the original operator, it becomes an eight-adjacent operator, as shown in Fig. 1(b). According to the different definitions of second-order differential, find the inverse of the numbers in the above two templates, and then Fig. 1(a) and Fig. 1(b) can be transformed into the form of Fig. 1(c) and Fig. 1(d). As you can see from the template, if a bright spot appears in a dark area of an image, the Laplacian operation will make the bright spot brighter [18-19]. Since the edges in an image are the areas where the gray value change, the Laplacian template can perform effective edge detection.

(a) (b) (c) (d)

Fig. 1. Laplace template

2.2 Gray Value Star-shaped Radiation Projection

In order to increase the gray value difference between each pixel and its adjacent pixels under strong illumination, this paper proposes a gray value star-shaped radiation projection method to describe the gray value information. In the gray value star-shaped radiation projection method, a central pixel point and a range of pixel points around it are selected as the area to be detected. The features are obtained by eliminating the false features and the noise points in the center points of the areas to be detected. Generally, the gray values of the center points in the detection areas containing features are larger, and that in the detection areas containing false features and the noise points are smaller. so the center point detection threshold can be set, and the detection areas containing false features and the noise points are eliminated by the gray value of the center point, which is a good way to improve the detection efficiency of the algorithm. The edge width extracted by the Laplace algorithm is 3 pixels, and a feature is the intersection of two edges, so we set the detection area size to 7*7, as shown in the gray area in Fig. 2. In

the detection area, each pixel is defined as a point (x, y, g) in a three-dimensional space, denoted as P (x, y, g), where (x, y) is the coordinate of point P. The coordinate of the detection center is (0, 0), and g is the gray value corresponding to each pixel. The gray value is projected from the detection center to 24 points on the edge of the detection area, and 24 projection lines are made from the center to the edge, and each line passes through four pixels. Add up the gray values of 4 pixels on each line to produce 24 projection values, such as $G_1 = g(0,0) + g(-1,1) + g(-2,2) + g(-3,3)$, $G_2 = g(0,0) + g(-1,1) + g(-1,2) + g(-2,3)$. All the projection values are to be compared, and all projection lines pass through the point (0, 0), so it is not necessary to accumulate the value of $g(0,0)$ when calculating the projection value.

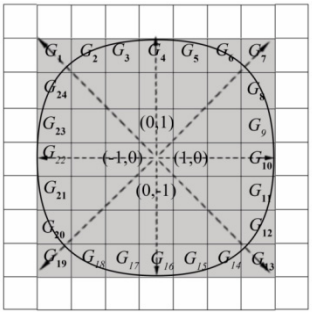

Fig. 2. Gray value star-shaped radiation projection of detection area

2.3 Locating Center Point

According to the difference of the gray value of features and false features, the sum of the projection values of the detection area corresponding to the features is larger, so the comparison threshold th_1 can be set. Firstly, calculate the sum of the projection values by the formula (4), shown as Vs, then compare the value of Vs with th_1 by the formula (5). If the value of Vs is larger than or equal to the value of th_1, the center point may be a features. Otherwise, the extraction of the center point is excluded.

$$Vs = \sum_{i=1}^{24} Gi = \sum_{i=1}^{24} \sum_{j=0}^{3} g(x,y). \tag{4}$$

$$fc = \begin{cases} 1, Vs >= th1 \\ 0, Vs < th1 \end{cases}. \tag{5}$$

Wherein, Vs is the sum of the projection values of a detection area, and th_1 is a comparison threshold. fc is a judgment result of whether the following detection should be performed for this point.

The comparison threshold th_1 is calculated as follows:

Step 1. Use the formula (4) to perform the gray value star-shaped radiation projection in all the areas to be detected, and calculate the sum of the projection values of each area.

Step 2. Calculate the average of the sum of the projection values of all the areas to be detected, and set the value to be the initial value of th_1.

Step 3. Use formula (5) to judge each area to exclude the false feature areas to reduce the number of areas to be detected.

Step 4. Repeat Step 2 and Step 3 to iterate the new value of th_1 and new areas to be detected. Set the iterations to be 10.

Through the above process, the number of areas to be detected is reduced. The features are usually located at the corner, so the center points of the straight lines need to be excluded. The false features may be extracted in the center points of the thick lines, so the image contour needs to be thinned.

Thinning the contour of the image means deleting the pixels of the contour as much as possible while ensuring the connectivity of the contour, and finally obtaining a contour of a single pixel width. In this paper, eight elimination templates are used to delete the pixels, as shown in Fig. 3. To prevent excessive deletion, two retention templates are designed, as shown in Fig. 4. In the figures, "1" represents the black

pixel in a binary image, and “0” represents the white pixel in a binary image, and “x” represents “0” or “1”.

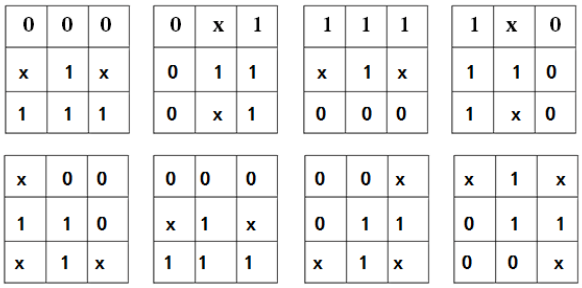

Fig. 3. Eliminating template

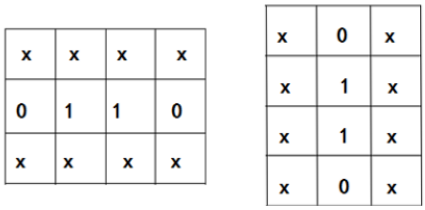

Fig. 4. Retention template

For each target pixel in the image, the adjacent 8 pixels are compared with all the elimination templates, and if they do not match, the pixel is retained. If it matches one of the elimination templates, match it with the retention template. If the matching is unsuccessful, this pixel is eliminated, otherwise this pixel is retained. Repeat the above process until the image no longer changes [20-21].

2.4 Judging the Main Peak Area

After the center points of the feature areas are pre-detected, they need to be optimized to eliminate the influence of noise points and filter out the false features of misjudgment. In this section, all the gray projection values of the retained feature areas are calculated, and the changes of the projection value of the areas can be observed. Generally, the projection value of feature changes greatly, but that of false feature changes little. According to this assumption, an algorithm for filtering false features adaptively is designed, described as follows:

(1) Display the projection values in the retained feature areas in the coordinate plane. The abscissa of the coordinate plane is the number of 24 directions, and the ordinate is the projection value on the corresponding number.

(2) Calculate the mean value of the projection value in the area.

(3) In order to highlight the characteristic that the projection value fluctuates greatly in feature areas, the filtering threshold can be set. The filtering threshold is set to 1.5 times or 2 times than mean value to achieve a better filtering effect. The higher the threshold is set, the lower the sensitivity of the feature is.

(4) Compare all the projection values with the threshold value. If there is a projection value larger than the threshold value, it is more likely that the center point of the area is a feature, and the area is determined to be the area where the main peak exists. For example, the projection values of an area are (12, 13, 14, 20, 38, 18, 11, 10, 48, 56, 24, 9, 9, 28, 54, 47, 26, 19, 11, 14, 2, 2, 0, 10), and the average value of the projection value is 20.625. The threshold is 30.937 when the threshold is 1.5 times the average, and the threshold is 41.25 when the threshold is 2 times the average. As shown in Fig. 5, there are projection values larger than the threshold, therefore, it is determined that this area is the main peak area.

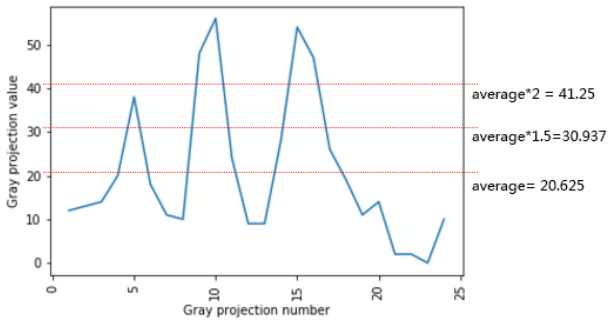

Fig. 5. Main peak area

2.5 Feature Extraction by Main Peak Distance

After the main peak areas are found, there is a possibility that a feature exists in the area. In the main peak area, the number of projection values greater than or equal to the threshold is obtained. If it is less than 2, this area is discarded. If it is greater than or equal to 2, the two largest projection values are found, and then the subtraction operation is performed. The result of subtraction is the main peak distance. It is observed that when the main peak distance is greater than or equal to 15 or less than or equal to 11, the main peak area is a feature area.

2.6 Generating Feature Rotation Invariance Descriptors

The BRIEF descriptor is used to perform feature description, and some pixel pairs around the feature can be selected. Comparing the gray value of each pair of pixels, a binary feature descriptor is formed by combining and coding. This method is simple, fast, and has the characteristic of rotation invariance [22-23]. The schematic of the BRIEF descriptor is shown in Fig. 6. In the schematic, four pixel pairs are selected around the feature P, and the comparison results of the four point pairs are combined as a descriptor. The algorithm is described as follows:

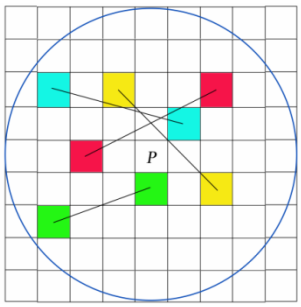

Fig. 6. Schematic of the BRIEF descriptor

Step 1. Define the descriptor piecewise function as τ in the $S \times S$ image area. The center point of this area is the feature P.

$$\tau(p;\quad x,\quad y)=\begin{cases}1, p(x)<p(y)\\0, p(x)\geq p(y)\end{cases}. \tag{6}$$

In formula (6), $p(x)$ is the gray value function.

Step 2. In the image area, select n pixel pairs like (x,y), and calculate the function value of formula (6) to generate the descriptor of the n-dimensional binary code. The calculation method of binary code is shown in formula (7).

$$f_n(p)=\sum_{1\leq i\leq n}2^{i-1}\tau(p;x_i,y_i). \tag{7}$$

In formula (7), the value of n is 128.

Step 3. Add the direction information of the feature descriptor. The direction of the offset vector between the gray value of the feature and the centroid is defined as the direction of the feature, and then the direction information of the feature is added to the descriptor. At any position (x_i, y_i), define a matrix Q of $2 \times n$.

$$Q = \begin{pmatrix} x_1, & x_2, & \cdots, & x_n \\ y_1, & y_2, & \cdots, & y_n \end{pmatrix}. \tag{8}$$

In formula (8), (x_i, y_i) represents any one of the pixel pairs.

The matrix corresponding to the feature direction θ is R_θ, and the pixel pair matrix constructed using R_θ is:

$$Q_\theta = R_\theta Q. \tag{9}$$

The feature descriptor after adding the direction is:

$$g_n(p, \theta) = f_n(p) \mid (x_i, y_i) \in Q_\theta. \tag{10}$$

Step 4. Using the greedy search method, the pixel pairs are constrained and the correlation of pixel pairs in the descriptor generated by formula (10) is reduced, thereby reducing the matching difficulty.

2.7 Feature Matching using Hamming Distance

The feature descriptor is in the form of binary code string, so the Hamming distance can be used to implement feature matching. Find the shortest and the second shortest Hamming distance between two feature descriptors. When the ratio of two Hamming distances is less than 0.8 and the Hamming distance is less than 50, the two features are determined to be matched [24-25].

3 Experiment and Data Analysis

The experimental environment of this paper was Intel i7 2.5 GHz CPU, windows system, openCV3.0, VC++ platform, and a monocular camera. The camera was used to capture video with a resolution of 640*480 and a frame rate of 30. First, a video was taken in the natural scene, and a comparison was made among the proposed algorithm in this paper, the improved SURF algorithm and the improved ORB algorithm on the performance of real-time; Second, the “COIL-100” image set [26] was used to verify the performance of visual angle variation; Third, the “ALOI” image set [27] was used to verify the performance of illumination variation. Finally, the video taken in the natural scene was used to verify the performance of scale variation.

3.1 Real-time Experiment

Augmented reality learning system has high requirements for real-time extraction and matching of features. Real-time performance is the most important evaluation factor for the performance of application system, and also is the purpose of the proposed algorithm in this paper. Therefore, real-time experiments on this algorithm are needed. A video was taken in the natural scene, and key frames of it were sampled, and the time taken in feature extraction in each key frame was calculated. In this experiment, a 55s video was taken in a natural scene, and a key frame were sampled every 40 frames. Finally, a total of 42 sample frames were acquired. The features of the 42 sample frames were extracted with improved SURF algorithm, improved ORB algorithm and algorithm in this paper respectively. The time used for feature extraction of each sample frame was recorded, and the comparison of feature extraction time of different algorithms was shown in Fig. 7. It can be seen that the improved SURF algorithm takes the most time, followed by improved ORB algorithm. The algorithm proposed in this paper take the least time.

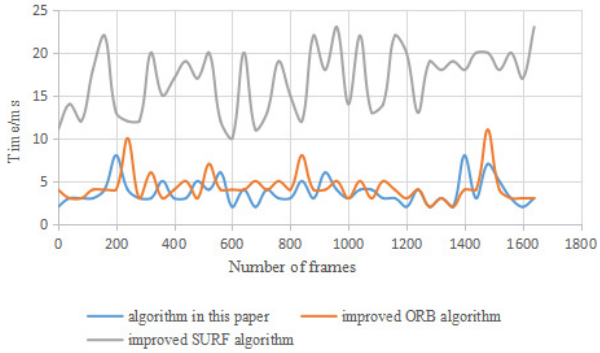

Fig. 7. The comparison of feature extraction time of different algorithms

The average time used to extract features by different algorithms was calculated respectively. The comparison results are shown in Table 1. The data results show that the proposed algorithm in this paper takes the least time in the feature extraction in the video frame sequence, which is only 22% of the improved SURF algorithm and 87% of the improved ORB algorithm. Therefore, it can better meet the real-time requirement of the augmented reality system.

Table 1. Average time used for features extraction of three algorithms

Algorithm	t/ms
improved SURF algorithm	16.82
improved ORB algorithm	4.28
algorithm in this paper	**3.72**

3.2 Visual Angle Variation Experiment

In order to verify the matching performance in case of visual angle variation in the algorithm proposed in this paper, 10 groups of object images were selected in the "COIL-100" image set, and each group contained 13 test images with different visual angle from 0 to 120 degrees. An image with a visual angle of 0 degree was used as a matching reference image. The improved SURF algorithm, the improved ORB algorithm and the algorithm proposed in this paper were used to match the reference image with the 13 test images in each group. Taking the obj80 in the "COIL-100" image set as an example, the matching results of the three algorithms with the visual angle of 0 degree, 40 degrees, and 120 degrees are shown in Fig. 8.

For the 10 groups of objects, 130 images were selected in the "COIL-100" image set, and the number of matching pairs, the number of correct matching pairs and the correct matching rate were calculated by the improved SURF algorithm, the improved ORB algorithm and the algorithm proposed in this paper respectively. Correct matching rate = the number of correct matching pairs / the number of matching pairs. The results of the number of matching pairs, the number of correct matching pairs, and the correct matching rate are shown in Table 2. The improved SURF algorithm has the largest number of matching pairs, but the correct matching rate is the lowest, so its matching performance is poor. The correct matching rate of the improved ORB algorithm is the highest, but the number of matching pairs is very small. During the experiment, it was found that there were a lot of matching results like the performances in Fig. 7(e) and Fig. 7(h). The matching performance of the improved ORB algorithm decreases rapidly when the visual angle changed. The improved ORB algorithm is not applicable to the matching task in the case of angle variation. Compared with the improved SURF algorithm, the matching performance of the algorithm proposed in this paper has great improvement. Both its matching number and correct matching number are significantly improved, therefore, the proposed algorithm in this paper is more suitable for the matching under the variation of visual angle.

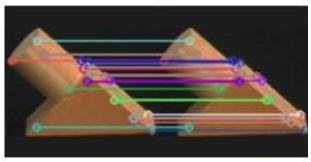

(a) improved SURF with the visual angle of 0 degree

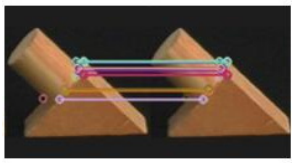

(b) improved ORB with the visual angle of 0 degree

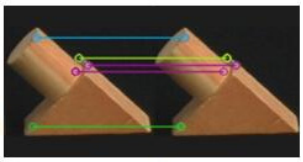

(c) algorithm proposed in this paper with the visual angle of 0 degree

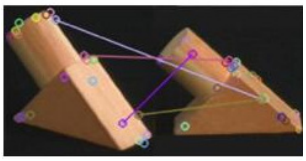

(d) improved SURF with the visual angle of 40 degrees

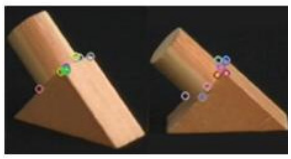

(e) improved ORB with the visual angle of 40 degrees

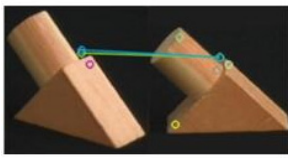

(f) algorithm proposed in this paper with the visual angle of 40 degrees

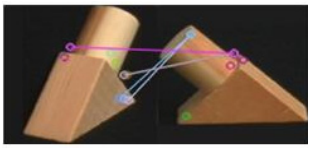

(g) improved SURF with the visual angle of 120 degrees

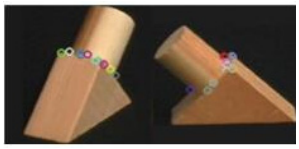

(h) improved ORB with the visual angle of 120 degrees

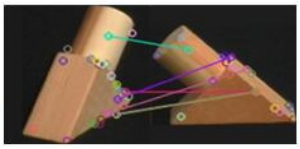

(i) algorithm proposed in this paper with the visual angle of 120 degrees

Fig. 8. Matching results with different visual angle using three algorithms

Table 2. Comparison of matching experiment data for the three algorithms with visual angle variation

algorithm	the number of matching pairs	the number of correct matching pairs	correct matching rate
improved SURF algorithm	**1040**	244	0.234
improved ORB algorithm	264	237	**0.898**
This paper's algorithm	622	**458**	0.736

3.3 Illumination Variation Experiment

In order to verify the matching performance of the algorithm proposed in this paper in the condition of illumination variation, 10 groups of different object images were selected in the "ALOI" image set. Each group contained 3 pictures of the object in conditions of different illumination intensity. The image with the normal illumination intensity was used as the reference image. The images under the conditions of poor illumination and strong illumination were used as the test images. The improved SURF algorithm, the improved ORB algorithm and algorithm proposed in this paper were used to match the reference image with the test images in each group. Taking the first group of pictures in the "ALOI" image set as an example, the matching results of test image with the reference image using the three algorithms under poor illumination and strong illumination conditions are shown in Fig. 9.

(a) improved SURF algorithm in the condition of poor illumination

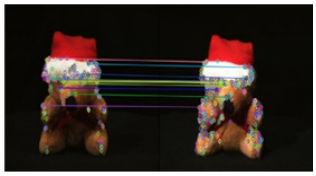

(b) improved ORB algorithm in the condition of poor illumination

(c) algorithm proposed in this paper in the condition of poor illumination

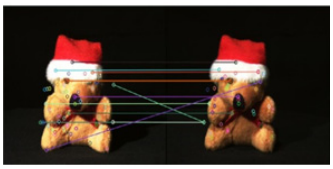

(d) improved SURF algorithm in the condition of strong illumination

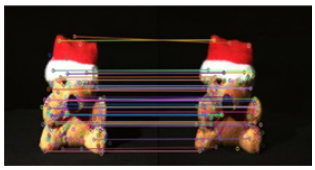

(e) improved ORB algorithm in the condition of strong illumination

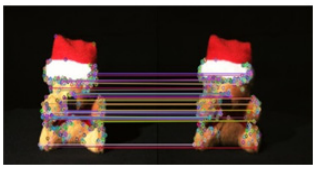

(f) algorithm proposed in this paper in the condition of strong illumination

Fig. 9. Matching results with different illumination intensity using three algorithms

For the 10 groups of objects, 130 images were selected in the "ALOI" image set, and the number of matching pairs, the number of correct matching pairs and the correct matching rate were calculated using the improved SURF algorithm, the improved ORB algorithm and the algorithm proposed in this paper respectively. The statistics and calculation methods were the same as that described in section 3.2. The results of the number of matching pairs, the number of correct matching pairs, and the correct matching rate are shown in Table 3.

Table 3. Comparison of matching experiment data for the three algorithms with illumination variation

algorithm	the number of matching pairs	the number of correct matching pairs	correct matching rate
SURF algorithm	405	339	0.837
ORB algorithm	**577**	**534**	0.925
This paper's algorithm	542	529	**0.976**

It can be seen that the improved ORB algorithm has the highest number of matching pairs in the condition of illumination variation in Table 3, but the correct matching rate of it is lower. The number of matching pairs in algorithm proposed in this paper is lower than that in the improved ORB algorithm, but its correct matching rate is the highest. The improved SURF algorithm has the lowest correct matching rate. The algorithm in this paper could magnify the difference in gray value information between each pixel and its adjacent pixels under different illumination conditions, therefore, the matching performance of the algorithm proposed in this paper has great improvement. In the case of illumination variation, the algorithm proposed in this paper has better robustness and the highest correct matching rate.

3.4 Scale Variation Experiment

In the video described in 3.1, different scales were added to the frames from the 1600th frame to the 1700th frame, which were used as the test image. The 0th frame was used as the reference image. The 0th frame and the 1600th frame were shown in Fig. 10. The improved SURF algorithm, the improved ORB algorithm and the algorithm proposed in this paper were respectively used to calculate the matching pairs, the correct matching pairs and the correct matching rate between the test picture and reference pictures. The statistics and calculation methods were the same as that described in Section 3.2. The statistical results are shown in Table 4.

(a) the 0th frame (reference image)

(b) the 1600th frame (test image)

Fig. 10. Effect of scale variation

Table 4. Comparison of matching experiment data for the three algorithms with scale variation

algorithm	the number of matching pairs	the number of correct matching pairs	correct matching rate
improved SURF algorithm	**1275**	741	0.581
improved ORB algorithm	1046	692	0.661
This paper's algorithm	977	**759**	**0.776**

It can be seen that when performing the scale variation experiment, the improved SURF algorithm has the most matching pairs in Table 4, but its correct matching rate is the lowest. The algorithm proposed in this paper has the least matching pairs, but its correct matching rate is the highest. The correct matching rate of the improved ORB algorithm is the second. Therefore, the matching performance of the algorithm proposed in this paper is more stability under the condition of scale variation.

3.5 Robustness Analysis

In order to analyze the robustness of this algorithms, correct matching rate, error matching rate and missing matching rate are calculated in case of angle variation, illumination variation, scale variation, and the results are shown in Table 5. We found the improved orb algorithm has the highest correct matching rate and the lowest missing matching rate in the case of angle variation, and the error matching rate of the algorithm proposed in this paper is the lowest, and it performs well in correct detection rate and error detection rate; In the case of illumination variation and scale variation, the correct matching rate of the algorithm proposed in this paper is the highest and the missing matching rate is the lowest, and there is no significant difference in the error matching rate among the three algorithms. Therefore, compared with the improved orb algorithm and the improved surf algorithm, the algorithm proposed in this paper has the strongest robustness.

Table 5. Comparison of robustness of the three algorithms

conditions	correct matching rate			error matching rate			missing matching rate		
	improved SURF	improved orb	algorithm proposed in this paper	improved SURF	improved orb	algorithm proposed in this paper	improved SURF	improved orb	algorithm proposed in this paper
angle variation	0.542	**0.626**	0.603	**0**	0.078	0	0.458	**0.295**	0.397
illumination variation	0.636	0.224	**0.675**	0	0	0	0.364	0.775	**0.325**
scale variation	0.422	0.286	**0.584**	0	0	0	0.578	0.714	**0.417**

3.6 Application of the Algorithm Proposed in This Paper

We designed and realized an AR learning system using the algorithm proposed in this paper. The system can be used as an English learning APP for children, through the traditional paper books and modern AR technology can make learning more interesting and lively. Applying the algorithm proposed in this paper to the augmented reality system, a good test result is obtained, as shown in Fig. 10. It can be seen from Fig. 11 that both the tracking and matching effect and the user experience are good in the case of

illumination variation, scale variation and visual angle variation, which indicate that this algorithm has practicability and stability.

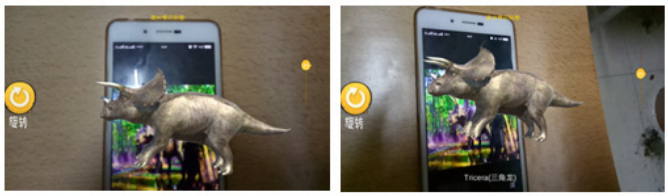

(a) matching effects of augmented reality system under illumination variation

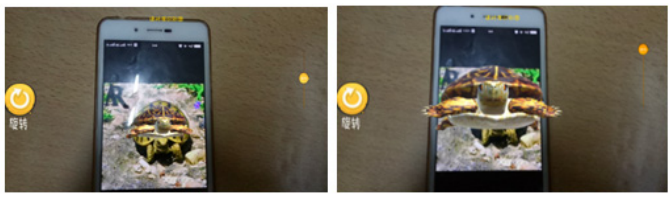

(b) matching effects of augmented reality system under scale variation

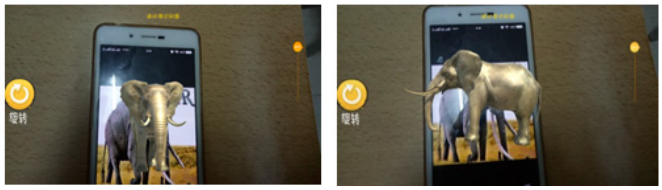

(c) matching effects of augmented reality system under visual angle variation

Fig. 11. Application effect of the algorithm proposed in this paper

4 Conclusions

In order to improve the performance of augmented reality systems in real-time, scale invariance and rotation invariance and meet the needs of special education fields, this paper proposes a feature extraction algorithm based on gray value star-shaped radiation projection. On the basis of extracting the edge of the image, this algorithm calculates the star-shaped projection value of all the pixels in the detection area to extract the features. Then the false features are gradually eliminated through the judgment of the main peak area and the main peak distance of the projection value. The feature description is performed with the BRIEF descriptor and the feature matching is made with Hamming distance. The experimental results show that the average time of feature matching in the proposed method in this paper is only 22% of the improved SURF algorithm and 87% of the improved ORB algorithm. The correct matching rate of the features is higher than both improved SURF algorithm and improved ORB algorithm in the case of illumination variation, scale variation and visual angle variation. The algorithm proposed in this paper has a good tracking and matching effects, and performs well in the user experience, which effectively improves the performance of the augmented reality system.

Acknowledgments

The work was supported by the Science and Technology Development Program of Henan Provincial Science and Technology Department (Grant No.182102310040).

The work was supported by the Humanities and Social Sciences Program of the Education Department of Henan Province (Grant No. 2020-ZDJH-295).

The work was supported by National Natural Science Foundation of China (Grant No. 61807014)

The work was supported by the Fundamental Research Funds for the Central Universities (No. CCNU19QN039)

References

[1] S. Joachim, A.N. Smith, Augmented reality: designing immersive experiences that maximize consumer engagement, Business Horizons 59(2)(2016) 149-161.

[2] I.-J. Lee, C.-H. Chen, C.-P. Wang, Augmented reality plus concept map technique to teach children with ASD to use social cues when meeting and greeting, The Asia-Pacific Education Researcher 3(2018) 1-17.

[3] J.A. Kosmicki, V. Sochat, M. Duda, Searching for a minimal set of behaviors for autism detection through feature selection-based machine learning, Transl Psychiatry 5(2)(2015) e514.

[4] A. Bellarbi, Toward mobile immersion in augmented reality: an approach based on robust natural feature tracking and 3D interaction, [dissertation] Paris: University of Paris-Saclay, 2017.

[5] S.A. Bakar, M.S. Hit, N.J. Wan, Improved global and gocal curvature properties for shape corner detection, Journal of Applied Sciences 17(9)(2017) 458-466.

[6] G. Ju, L. Yuan, X.-Y. Liu, H.E. Yue, Study on mobile target real-time image registration based on improved SURF algorithm, Journal on Communications 38(2017) 177-186.

[7] W.-S. Gong, S.-L. Zhou, X.-Z. Wu, ORB-SLAM method based on improved FAST feature detection, Modern Electronics Technique 41(6)(2018) 53-56.

[8] M. Trajković, M. Hedley, Fast corner detection, Image and Vision Computing 16(2)(1998) 75-87.

[9] S. Park, G. Kim, J. Park, A 1.5nJ/pixel super-resolution enhanced FAST corner detection processor for high accuracy AR, in: Proc. the 40th European Solid State Circuits Conference, 2014.

[10] L.-F. Wu, Y. Gao, J.-W. Zhang, An improved SIFT algorithm based on FAST corner detection, in: Proc. 2013 the 9th International Conference on Intelligent Information Hiding and Multimedia Signal Processing, 2013.

[11] W.-C. Zhang, X.-N. Kong, W. Song, Review of image corner detection algorithms, Acta Electronica Sinica 43(11)(2015) 2315-2321.

[12] D.G. Lowe, Distinctive image features from scale-invariant keypoints, International Journal of Computer Vision 60(2)(2004) 91-110.

[13] H. Bay, A. Ess, T. Tuytelaars, Speeded-up robust features, Computer Vision & Image Understanding 110(3)(2008) 404-417.

[14] E. Rublee, V. Rabaud, K. Konolige, ORB: an efficient alternative to SIFT or SURF, in: Proc. IEEE International Conference on Computer Vision, 2012.

[15] F. Yan, C.-J. Zhou, Y.-T. Tian, Image edge points detection algorithm for object localization, Journal of Jilin University, 46(2016) 2103-2110.

[16] R.-L. Duan, Q.-X. Li, Y.-H. Li, Summary of Image Edge Detection, Optical Technique, 2005.

[17] I. Agustina, F. Nasir, A. Setiawan, The implementation of image smoothing to reduce noise using Gaussian filter, International Journal of Computer Applications 177(5)(2017) 15-19.

[18] D. Hazarika, V. K. Nath, M. Bhuyan, SAR image despeckling based on combination of laplace mixture distribution with local parameters and multiscale edge detection in lapped transform domain, Procedia Computer Science 87(2016) 140-147.

[19] L. Zhang, Z.-C. Wu, Y.-G. Wang, Laplacian line drawing algorithm based on difference-of-Gaussian approximation, Journal of Computer-Aided Design & Computer Graphics 27(10)(2015) 1936-1943.

[20] B. Pauland, D. Ghoshal, An improved study on edge based image segmentation and subsequent edge thinning, Indian Journal of Science & Technology 9(44)(2016).

[21] C. Zhang, W. Zhong, C. Zhang, Simulation design of improved OPTA Thinnin algorithm, in: Proc. International Conference on Mechatronics and Intelligent Robotics, 2017.

[22] T. Chen, F. Wang, Real-time robust feature-point matching algorithm, Journal of Image & Graphics, 2016. https://en.cnki.com.cn/Article_en/CJFDTotal-ZGTB201609010.htm

[23] L. Li, Objects feature match algorithm based on image structure and improved brief detector, Foreign Electronic Measurement Technology 36(2)(2017) 29-33.

[24] R. Liu, D. Peng, Y. Liu, Research and implementation of image feature matching method based on OpenCV, in: Proc. International Conference on Advances in Mechanical Engineering and Industrial Informatics, 2016.

[25] M. Tahir, N. Kanwal, F. Anjum, FAB: fast angular binary descriptor for matching corner points in video imagery, Journal of Robotics 2016(1)(2016) 1-11.

[26] S.A. Nene, S.K. Nayar, H. Murase, Columbia object image library (COIL-100), Columbia University, 1996.

[27] J.M. Geusebroek, G.J. Burghouts, A.W. Smeulders, The Amsterdam library of object images, International Journal of Computer Vision 61(1)(2005) 103-112.